Asymmetric Synthesis of S(IV)-Stereogenic Sulfinimidate Esters by Sulfinamide Activation

Qiang Xiong,[a] Minghong Liao,[a] Sha Zhao,[a] Sitian Wu,[a] Ya Hong,[a] Yonggui Robin Chi,[a][b] Xinglong Zhang,[c]* Xingxing Wu[a]*

[a] State Key Laboratory of Green Pesticide, Key Laboratory of Green Pesticide and Agricultural Bioengineering, Ministry of Education, Guizhou University, Huaxi District, Guiyang 550025, China.
[b] School of chemistry, chemical engineering, and biotechnology, Nanyang Technological University, Singapore 637371, Singapore
[c] Department of Chemistry, The Chinese University of Hong Kong, Shatin, New Territories, Hong Kong, China

*Corresponding author. Email: wuxx@gzu.edu.cn; xinglong.zhang@cuhk.edu.hk

Table of Contents

2.7 Preliminary mechanistic studies

Scheme S21. Control experiment with protected catalyst Cat. **N**

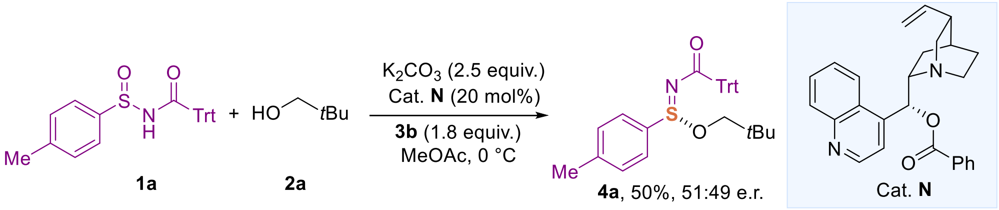

Control experiment was performed to shed insights into the role of hydroxyl groups on Cat. **E**. As illustrated in Scheme S21, using benzoyl-protected Cat. **N** instead of Cat. **E**, the product **4a** was obtained in similar yields, but the enantioselectivity decreased sharply (compared with Table S5, entry 3 with Cat. **E**: 73%, 96:4 e.r.), indicating that the hydroxyl group was crucial to the enantioselectivity control of the sulfinimidate ester product **4**.

Experimental procedure: A solution of **1a** (12.8 mg, 0.03 mmol, 1.0 equiv.), Cat. **N** (1.8 mg, 0.006 mmol, 20 mol%), **3b** (11.8 mg, 0.054 mmol, 1.8 equiv.), K_2CO_3 (10.4 mg, 0.75 mmol, 2.5 equiv.) and **2a** (1.0 M in MeOAc, 0.15 mmol, 1.5 equiv.) in MeOAc (0.3 mL) were stirred at 0 °C for 6 days. Yield of **4a** was determined by ^{1}H NMR spectroscopy, based on **1a**, by using 1,3,5-trimethoxybenzene as an internal standard. Enantiomeric ratio (e.r.) was determined by high-performance liquid chromatography (HPLC) analysis.

Scheme S22. Isotopic labelling experiments and HRMS detection of sulfonate **^{18}O-16**

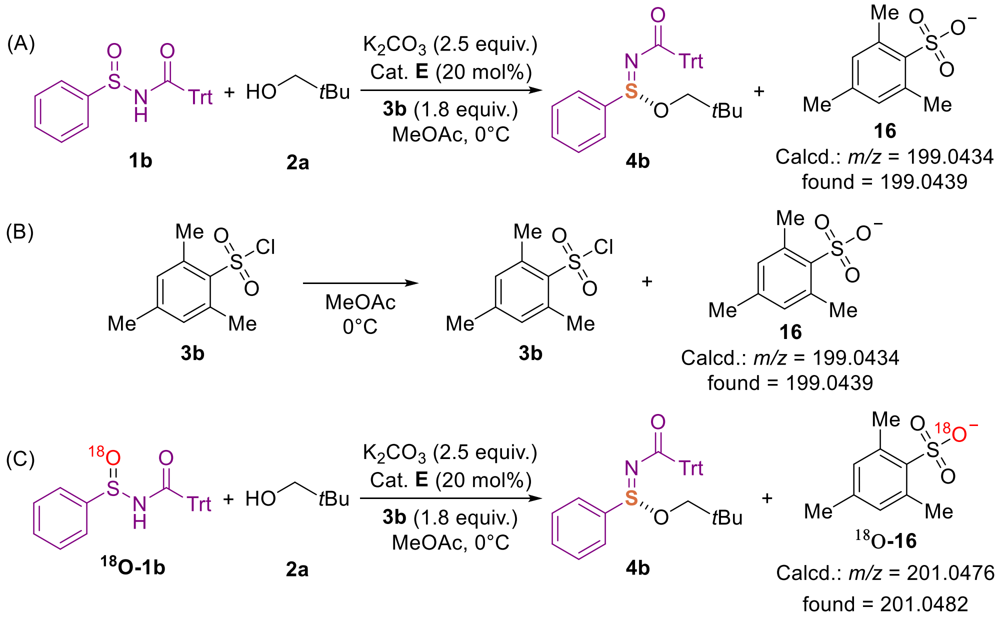

As illustrated in Scheme S18, to probe the reaction process we first successfully detected the existence of sulfonate anion **16** from the model reaction under the optimal conditions (Scheme S22A). Since the sulfonate **16** was also viable from the hydrolysis of the sulfonyl chloride (Scheme S22B), an ^{18}O-labelled sulfinamide **^{18}O-1b** was then prepared and subjected into the catalytic conditions. Accordingly, the detection of the ^{18}O-labelled sulfonate anion **^{18}O-16** could strongly support the proposed sulfinamide activation process (Scheme S22C).

Experimental procedure for eq. 1: To a stirred solution of **1b** (12.4 mg, 0.03 mmol, 1.0 equiv.), Cat. **E** (1.8 mg, 0.006 mmol, 20 mol%), **3b** (11.8 mg, 0.054 mmol, 1.8 equiv.) and K_2CO_3 (10.4 mg, 0.75 mmol, 2.5 equiv.) in MeOAc (0.3 mL) were added dropwise **2a** (1.0 M in MeOAc, 0.045 mmol, 1.5 equiv.) at 0 °C. After stirring for 48 h at 0 °C. The crude ESI-MS spectrometric was recorded (Figure S3).

Experimental procedure for eq. 2: **3b** (11.8 mg, 0.054 mmol, 1.8 equiv.) was dissolved in MeOAc (0.3 mL). The reaction mixture was stirred for 48 h at 0 °C. The crude ESI-MS spectrometric was recorded (Figure S4).

Experimental procedure for eq. 3: To a stirred solution of **^{18}O-1b** (12.4 mg, 0.03 mmol, 1.0 equiv.), Cat. **E** (1.8 mg, 0.006 mmol, 20 mol%), **3b** (11.8 mg, 0.054 mmol, 1.8 equiv.) and K_2CO_3 (10.4 mg, 0.75 mmol, 2.5 equiv.) in MeOAc (0.3 mL) were added dropwise **2a** (1.0 M in MeOAc, 0.045 mmol, 1.5 equiv.) at 0 °C. After stirring for 48 h at 0 °C. ^{18}O incorporation was observed in product **^{18}O-16** by ESI-MS spectrometric analysis (Figure S5).

Scheme S23. HRMS detection of catalyst-bound reactive intermediate **II**

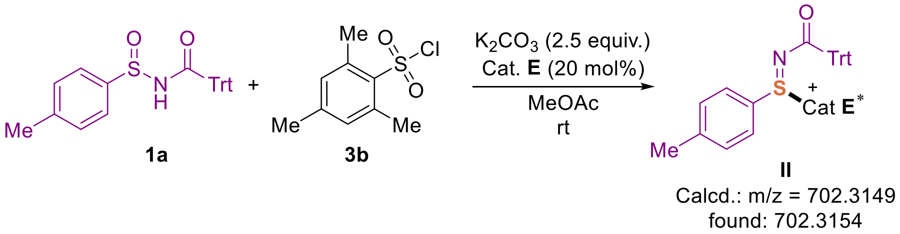

To detect the catalyst bound reactive species, we have performed the model catalytic reaction in the absence of alcohol (Scheme S23). As illustrated in Figure S6, HRMS successfully detected the existence of aza-sulfinyl ammonium intermediate **II** from the control experiment in Scheme S23, indicating that catalyst **E** was involved in the activation of the aza-sulfinyl mixed anhydride and enantioselective control process.

Experimental procedure: To a stirred solution of *N*-protected sulfinamide **1a** (12.4 mg, 0.03 mmol, 1.0 equiv.), Cat. **E** (1.8 mg, 0.006 mmol, 20 mol%), **3b** (11.8 mg, 0.054 mmol, 1.8 equiv.) in MeOAc (0.3 mL) were added K_2CO_3 (10.4 mg, 0.75 mmol, 2.5 equiv.). After stirring for 48 h at rt. The crude ESI-MS spectrometric was recorded (Figure S6).

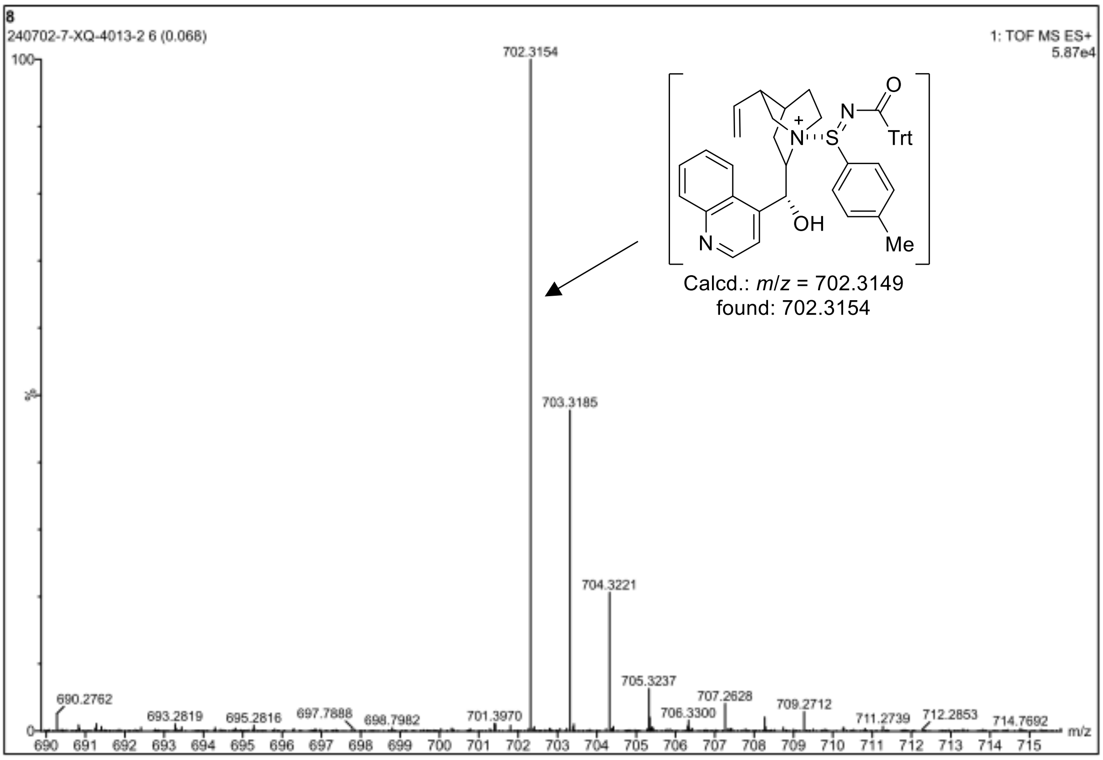

Figure S6. ESI-MS spectrum for crude reaction mixture of Scheme S23

Scheme S27. Plausible reaction mechanism

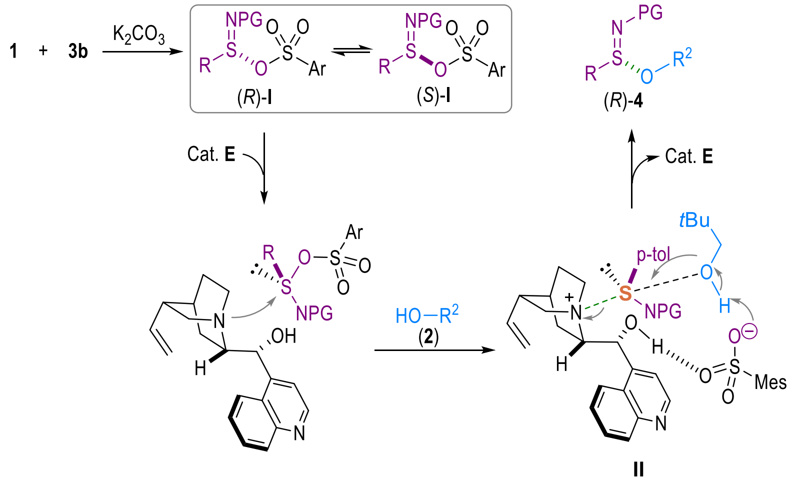

A plausible mechanism to account for the developed catalytic synthesis of chiral sulfinimidate scaffolds was illustrated in Scheme 27. Initially, the aza-sulfinyl mixed anhydride was readily formed through activation of the sulfinamide **1** by sulfonyl chloride **3b**. Subsequent S_N2 type displacement of the nucleophilic amine moiety of the catalyst to the S-center of the anhydride species **I** would give the key aza-sulfinyl ammonium intermediate **II**. Approach of alcohol nucleophiles from the back of S-N bond of **II** would afford the desired sulfinimidate products **4**, and regenerate the CD catalyst. Considering the pivotal role of the free hydroxyl group in the cinchonine catalyst and the DFT calculations on the transition state, an intermediate of **II** from catalyst addition of (*R*)-**I** was assumed to give rise to the product in high enantioselectivity.

3. Computational section

3.1 Conformational sampling

Conformational sampling of key reaction intermediates and transition states was carried out at GFN2-xTB[17–19] level of theory using the CREST program version 2.12 by Grimme and co-workers.[20,21] For transition states, key distances were constrained with a force constant of 0.25 a.u. as implemented in CREST program. The conformers and rotamers ensemble was generated using the iterative metadynamics based on genetic z-matrix crossing algorithm (iMTD-GC). Conformers were further optimized at GFN2-xTB level with very tight (*-opt vtight*) optimization. We then further chose 10 of the lowest energy conformers from each CREST sampling result to be further optimized at density functional theory (DFT) level of theory and used the conformer of the lowest DFT energy for full mechanistic studies and final potential energy surface (PES) Gibbs energy profile.

3.2 Density functional theory (DFT) calculations

DFT calculations were carried out using the *Gaussian 16* rev. B.01 program.37 The global hybrid functional M06-2X[38] with the def2-SVPD[6,7] Karlsruhe-family basis set for S and Cl atoms and def2-SVP[22,24] basis set for all other atoms (this mixed basis set is denoted BS1) was employed for all gas-phase optimizations. The "D" in def2-SVPD basis set denotes diffuse functions which are important for the correct description of anionic electron distributions.[25–27] The M06-2X functional was chosen for the study of the present system, as it has been employed in the studies of NHC organocatalysis with good accuracy.[28–37] Minima and transition structures on the potential energy surface (PES) were confirmed as such by harmonic frequency analysis, showing respectively zero and one imaginary frequency, at the same level of theory. Intrinsic reaction coordinate (IRC) analyses[38,39] were performed to confirm that the found TSs connect to the right reactants and products. In cases where the IRC did not succeed, presumably due to very flat PES around the TS region, quick reaction coordinate (QRC)[40] analysis (optimization of the structures at both ends of the TS vibrational normal mode identified by QRC displacement) was performed to confirm that the TS identified is indeed the desired one.

Single point (SP) corrections were performed using M06-2X functional with def2-TZVPD[22,23] basis set for S and Cl atoms and def2-TZVP[22,24] for all other atoms (denoted BS2). The SMD implicit continuum solvation model[40] was included to account for the solvent effect of methyl ethanoate. Gibbs energies were evaluated at 0°C temperature (reaction condition), using the entropic quasi-harmonic treatment scheme of Grimme,[42] at a cut off frequency of 100 cm^{-1}. The free energies were further corrected using standard concentration of 1 mol/L, which was used in solvation calculations. The free energies reported in Gaussian from gas-phase optimisation were further corrected using standard concentration of 1 mol/L,[41–43] which were used in solvation calculations, instead of the gas-phase 1atm used by default in Gaussian program. Data analysis was carried out using the GoodVibes code version 3.1.1.[44] Gibbs energies evaluated at SMD (methyl ethanoate)-M06-2X/BS2//M06-2X/BS1 level of theory is given in kcal/mol and used for discussion throughout. All molecular structures and molecular orbitals were visualized using *PyMOL* software.[45]

3.3 Model reaction

We chose the following reaction (entry 13, Scheme 1 of the main text) as our model system to study the catalytic mechanism of the formation of chiral sulfinimidate ester (Scheme S22). From experimental evidence, we envisioned that substrate **1a** and **3b** will react to form the aza-sulfinyl mixed anhydride **Ia**. From there, the chiral catalyst Cinchonidine (**CD**) may attack each of the enantiomer of **Ia**, via S_N2, to give epimeric forms of the aza-sulfinyl ammonium intermediate **IIa**, with different barrier heights. Finally, the alcohol nucleophile attacks the S-N bond of **IIa** in an S_N2 manner to yield the desired sulfinimidate product **4a** (overall retention of configuration resulting from sequential S_N2 steps). We studied the detailed mechanisms of these steps computationally.

Scheme S28. Model reaction used for computational studies.

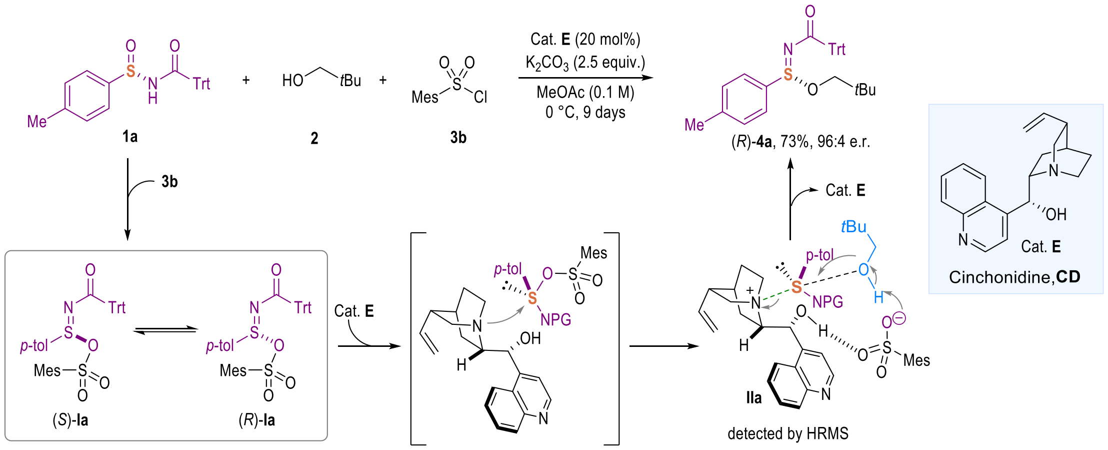

3.4 Racemization of aza-sulfinyl mixed anhydride

We performed DFT calculations to understand if the aza-sulfinyl mixed anhydride substrate, **Ia**, may racemize under the reaction conditions. Conformational sampling on intermediate **Ia** was performed as described in the methods section to locate 10 lowest DFT energy structures and the lowest energy structure of **Ia** was used subsequently. The mixed anhydride may undergo a trigonal planar transition state (TS), **TS$_{\mathbf{trig}}$**, that interconverts the two enantiomeric forms of this substrate. However, this TS has a very high barrier of 50.2 kcal/mol, which is unfeasible at the reaction temperature of 0 ºC. It was shown experimentally that the racemization can occur in the absence of the chiral catalyst Cinchonidine, thus, we need not consider the participation of the catalyst in the racemization step. The DFT optimized structure is shown in Figure S7.

Following the mechanism of anion-assisted racemization reported by Zhang and Wu,[37] coupled with the experimental evidence that using the optically enriched starting material (*S*)-**1a** *without addition of catalyst **E*** will yield racemic product **4a** (Scheme S20), we considered a similar mechanism for racemization with 2,4,6-trimethylbenzenesulfonate anion. Note that in that system,[37] we have tried locating the TS racemization via pseudorotation, but to no avail (we have also used true pseudorotational barrier for phosphorus system and Ni system[46] as a starting guess structure and modifying it to S chiral center but did not succeed in locating any such TS). The relaxed PES scan energy profile for the current system is shown in Figure S6. This shows that in the mixed anhydride, the S–O bond distance is 1.73Å (structure **1**).

There is a small barrier of complex formationlax, lland (~ 1 kcal/mol) as the sulfonate anion approaches intermediate **Ia**. This then yields a stable complex (structure **5**). Further shortening of the S–O bond length suggests that there may be a barrier of racemization of about 10 kcal/mol (S–O bond distance of 1.73 Å in structure **6** of Figure S6). Note that this PES scan gives an upper bound estimate for the putative TS and the actual TS barrier can be much lower.[46,47] The direct location of the TS for racemization has, however, been unsuccessful. Using the system where the trityl group is replaced by *tert-Bu* group, we were able to locate the TS for racemization, with a barrier of 2.9 kcal/mol, relative to the starting anionic complex between mixed anhydride and sulfonate anion. This TS, **TS$_{\text{rac}}$**, is shown in Figure S7.

TS$_{\text{trig}}$	**TS$_{\text{rac}}$**
$\Delta G^{\ddagger} = 50.2$	$\Delta G^{\ddagger} = 2.9$
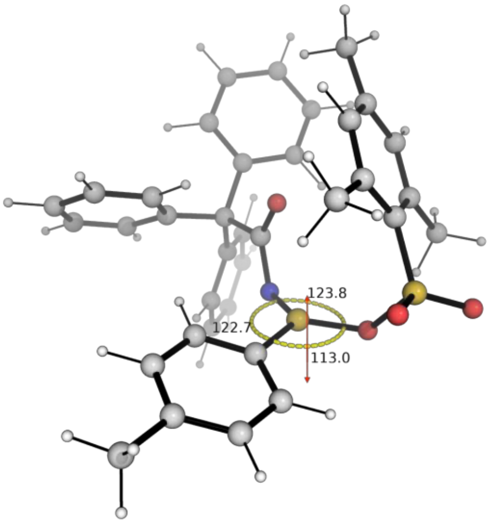	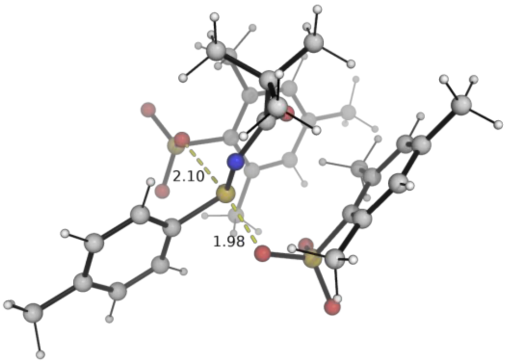

Figure S7. DFT-optimized structures of the transition states for the racemization of mixed anhydride. Key bond distances are given in Å and key angles are given in degrees. Red arrow indicates the vibrational mode for the inversion of sulfur atom in the TS. Activation barriers are in kcal/mol and taken relative to the mixed anhydride as zero reference for **TS$_{\text{trig}}$** and relative to the starting anionic complex for **TS$_{\text{rac}}$**.

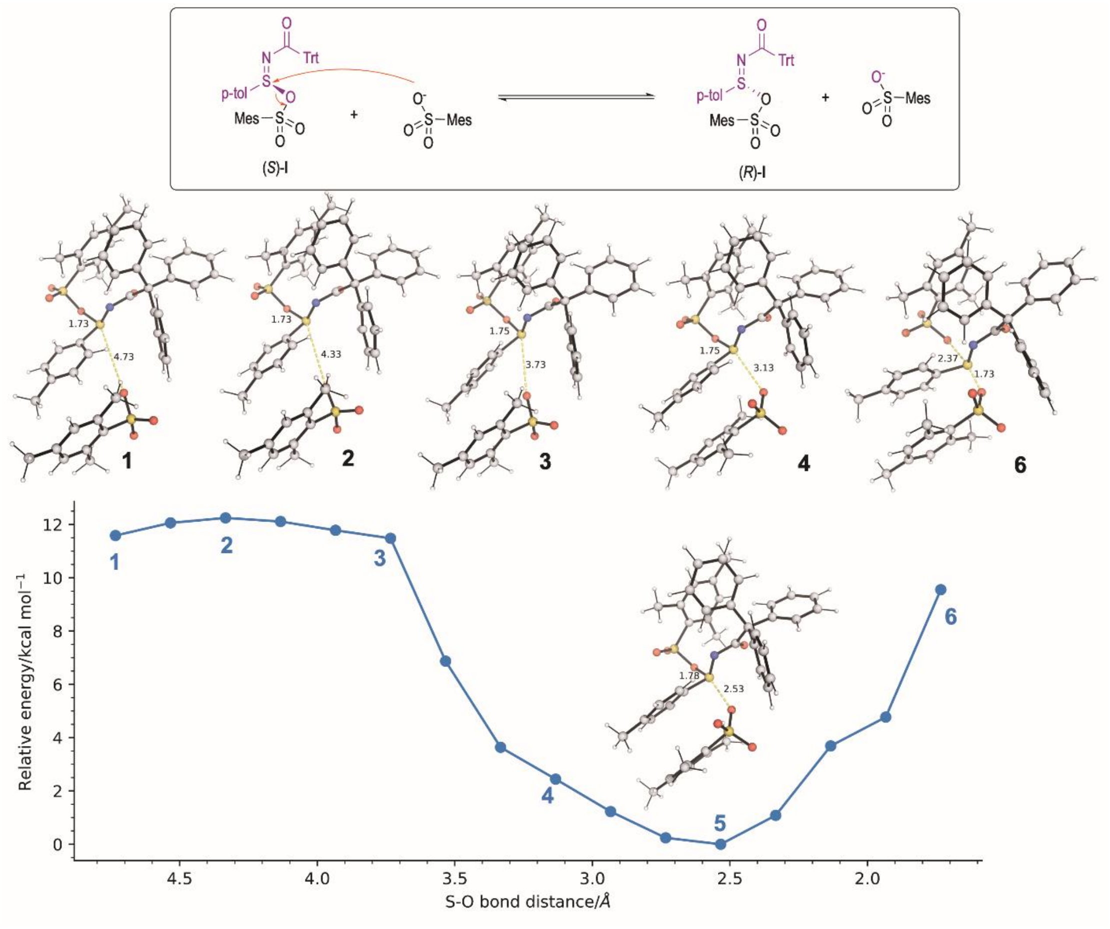

Figure S8. Relaxed potential energy surface (PES) scan along S–O distance in the gas phase.

3.5 Formation of catalyst-derived aza-sulfinyl ammonium intermediate

The feasibility of the attack of the mixed anhydride by the chiral **CD** catalyst was explored computationally. There seems to be no barrier for the formation of the aza-sulfinyl ammonium intermediate **IIa**, as the direct optimization of complex of catalyst **CD** and lowest energy conformer of **Ia** yields the ammonium intermediate. We tried locating the TS with direct TS search with implicit solvation and found this barrier to be 0.9 kcal/mol (verified by QRC;[40] see structures in *DFT_optimized_structures* folder). The complexation between catalyst **CD** and lowest energy conformer of (*R*)-**Ia** and (*S*)-**Ia** is reversible, with two complexes existing in equilibrium, governed by the Gibbs energy difference between **R_INT1** and **S_INT1** (Scheme 4D, main text). The resting state or the turnover-frequency (TOF) determining intermediate (TDI) for the whole catalytic cycle is thus **R_INT1**, as **R_INT1** and **S_INT1** can interconvert before the bond formation in the next step, via **TS2**.[48,49]

3.6 Product formation via nucleophilic attack on sulfinyl azolium intermediate

The nucleophilic attack on the ammonium intermediate by 2,2-dimethylpropan-1-ol was studied computationally. The DFT-optimized lowest energy TSs and their associated intermediates were shown in Figure S9. Only 5 lowest energy structures from CREST sampling were used as guess structures for TS search and we report only successfully located TSs using DFT. For some structures, the "modredundant" jobs succeeded but the actual TS search failed, for these, we used the resulting structure from the "modredundant" jobs to estimate the TS barrier. These structures end with "est", denoting "estimated". The comparison between the true TS structure and the "modredundant" structure show that they fall within 1 kcal/mol. In Figure S9, only the true TS structures are shown and the "estimated" structures are given in *DFT_optimized_structures* folder (they do not yield any TSs lower in energy than those true TSs located).

R_INT2	**R_TS2**
$\Delta G = -1.0$	$\Delta G^{\ddagger} = 1.2$

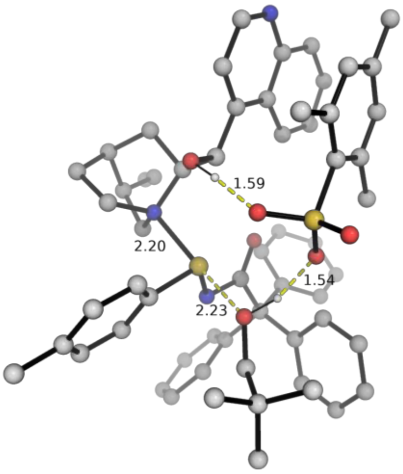

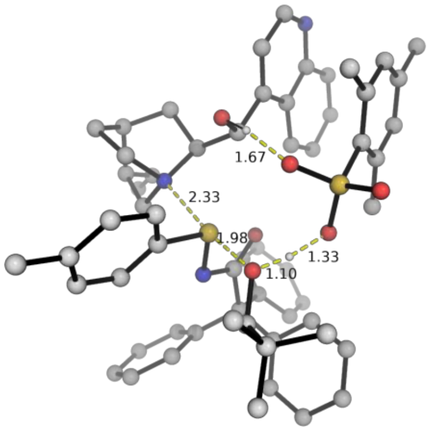

R_TS2-c2	**R_TS2-c3**
$\Delta G^{\ddagger} = 5.9$	$\Delta G^{\ddagger} = 6.0$

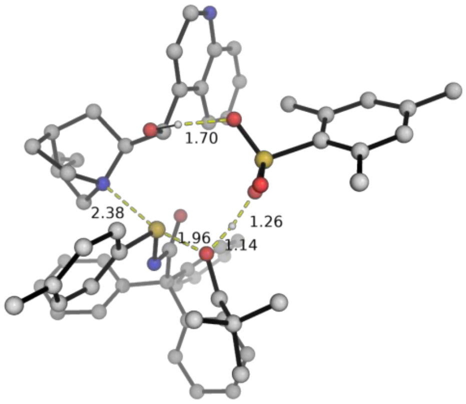

R_TS2-c4

ΔG‡ = 6.1

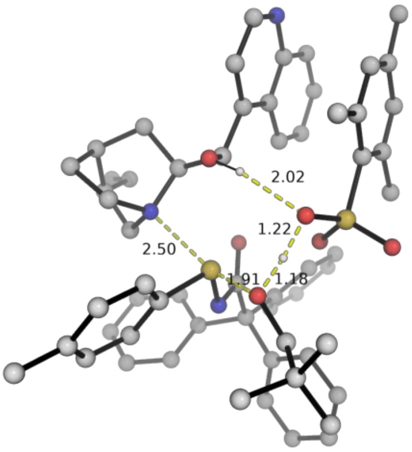

R_INT3

ΔG = -2.6

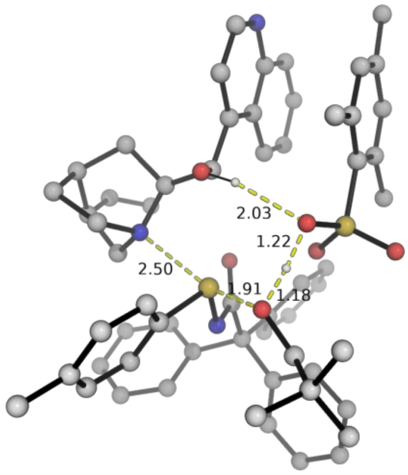

S_INT2

ΔG = -0.1

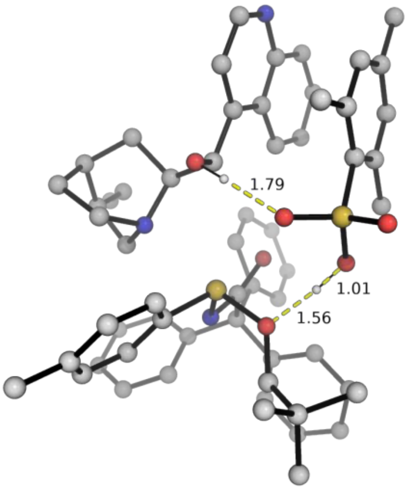

S_TS2

ΔG‡ = 3.9

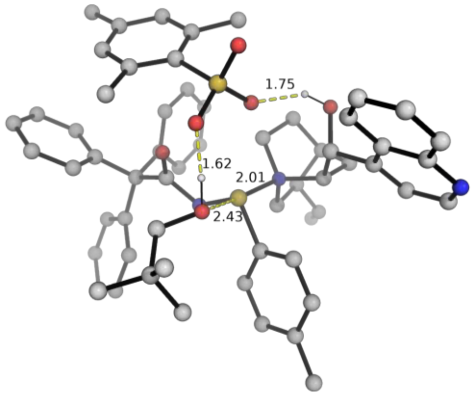

S_TS2-c2

ΔG‡ = 11.1

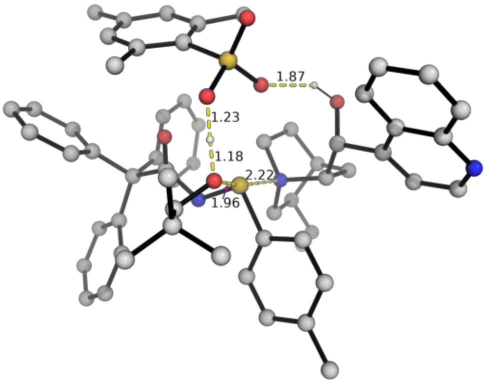

S_INT3

ΔG = -5.7

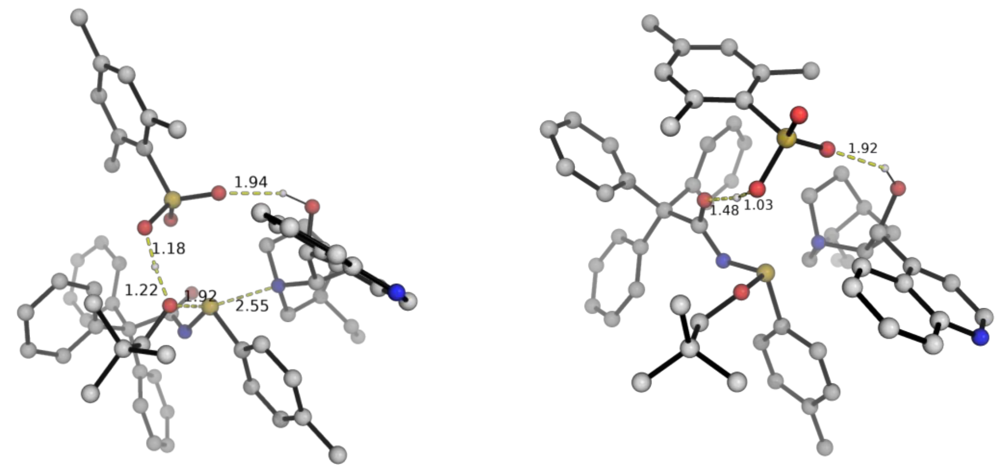

Figure S9. DFT-optimized structures of the lowest energy intermediates and transition states (TSs) for the product formation. Key bond distances are given in Å. Activation barriers and energies are in kcal/mol and taken relative to the mixed anhydride as zero reference.

3.7 Optimized structures and raw energy values

Geometries of all optimized structures (in.xyz format with their associated gas-phase energy in Hartrees) are included in a separate folder named *DFT_optimized_structures* with an associated readme.txt file. All these data have been uploaded to https://zenodo.org/records/13941543 (DOI: 10.5281/zenodo.13941543).

Absolute values (in Hartrees) for SCF energy, zero-point vibrational energy (ZPE), enthalpy and quasi-harmonic Gibbs free energy for M06-2X/BS1 optimized structures and single point corrections in SMD(methyl ethanoate) using M06-2X/BS2 functional are also included.

Structures	**E/au**	**ZPE/au**	**H/au**	**T.S/au**	**qh-G/au**	**SP SMD(methyl ethanoate) M06-2X/BS2**
1a	-1644.517978	0.434536	-1644.0597	0.075275	-1644.12833	-1646.073343
3a	-1357.492941	0.186194	-1357.2943	0.04628	-1357.338837	-1358.3988
HCl	-460.647762	0.006795	-460.63794	0.016461	-460.6544	-460.803965

2a	-272.636094	0.165097	-272.46327	0.032659	-272.49591	-272.960252
CD	-920.897077	0.381122	-920.50011	0.054312	-920.551878	-921.9362346
sulfonate_anion	-972.668649	0.187448	-972.46918	0.045847	-972.513018	-973.586115
sulfonic_acid	-973.183618	0.199301	-972.97166	0.046726	-973.016431	-974.0369118
prd_4a	-1840.815668	0.574896	-1840.2113	0.086978	-1840.29065	-1842.585918
prd_4a-c2	-1840.815668	0.574904	-1840.2113	0.086619	-1840.290471	-1842.585919
prd_4a-c3	-1840.815668	0.574878	-1840.2122	0.083315	-1840.28919	-1842.585918
prd_4a-c4	-1840.815036	0.57521	-1840.2105	0.086463	-1840.289376	-1842.583677
prd_4a-c5	-1840.810035	0.574676	-1840.2059	0.086656	-1840.28498	-1842.579572
prd_4a-c6	-1840.804382	0.574523	-1840.2003	0.0867	-1840.279503	-1842.576179
Ia	-2541.358915	0.609761	-2540.7152	0.094609	-2540.802394	-2543.649352
Ia-c2	-2541.358915	0.609767	-2540.7152	0.09455	-2540.802364	-2543.649355
Ia-c3	-2541.357583	0.609875	-2540.7138	0.09475	-2540.800891	-2543.648053
Ia-c4	-2541.355491	0.609615	-2540.7118	0.096188	-2540.799614	-2543.647224
Ia-c5	-2541.357073	0.609591	-2540.7136	0.095631	-2540.801217	-2543.647164
Ia-c6	-2541.357075	0.609827	-2540.7135	0.094648	-2540.800526	-2543.64713
Ia-c7	-2541.357075	0.609829	-2540.7135	0.094627	-2540.800515	-2543.64713
Ia-c8	-2541.355488	0.609529	-2540.7127	0.093808	-2540.798795	-2543.647219
Ia-c9	-2541.355885	0.609612	-2540.7123	0.095046	-2540.799541	-2543.645828
Ia-c10	-2541.355886	0.609637	-2540.7123	0.0948	-2540.799423	-2543.645826
Ia-c11	-2541.3571	0.609828	-2540.7143	0.091282	-2540.799213	-2543.647097
TS_trig	-2541.276363	0.607492	-2540.6349	0.096811	-2540.722819	-2543.566323

R_INT1	**-3462.301768**	**0.993451**	**-3461.2579**	**0.132667**	**-3461.377009**	**-3465.618018**
R_INT1-c2	-3462.301769	0.993494	-3461.2579	0.131816	-3461.376581	-3465.618017
R_INT1-c3	-3462.298925	0.992959	-3461.2553	0.133117	-3461.374724	-3465.616299
R_INT1-c4	-3462.298925	0.992966	-3461.2553	0.133028	-3461.374685	-3465.616303
R_INT1-c5	-3462.296814	0.99297	-3461.2535	0.129733	-3461.371563	-3465.612028
R_INT1-c6	-3462.296813	0.992974	-3461.2535	0.129727	-3461.371555	-3465.612022
R_INT1-c7	-3462.30038	0.993722	-3461.2565	0.130924	-3461.374672	-3465.610877
R_INT1-c8	-3462.30038	0.993742	-3461.2565	0.130721	-3461.374564	-3465.610882
R_INT1-c9	-3462.297793	0.993551	-3461.2539	0.130591	-3461.372035	-3465.609998
R_INT1-c10	-3462.297791	0.993461	-3461.2548	0.128216	-3461.371226	-3465.609992
R_INT1-c11	-3462.296893	0.993373	-3461.2535	0.128188	-3461.370595	-3465.608006
R_INT1-c12	-3462.296894	0.993376	-3461.2535	0.128183	-3461.37059	-3465.608003
R_INT1-c13	-3462.296894	0.993376	-3461.2535	0.128164	-3461.370582	-3465.608007
R_INT1-c14	-3462.296905	0.993299	-3461.2537	0.127634	-3461.370383	-3465.603893
R_INT1-c15	-3462.296905	0.993301	-3461.2537	0.12759	-3461.370364	-3465.6039
R_INT2	-3734.970417	1.160242	-3733.7528	0.145054	-3733.883867	-3738.592034
R_TS2	**-3734.970071**	**1.158813**	**-3733.7548**	**0.142189**	**-3733.883757**	**-3738.588332**
R_INT3	-3734.978108	1.160055	-3733.7616	0.141709	-3733.890357	-3738.595823
R_TS2-c2	-3734.953278	1.156959	-3733.739	0.146019	-3733.870379	-3738.577499

R_TS2-c3	-3734.96445	1.156531	-3733.751	0.141652	-3733.880405	-3738.57841
R_TS2-c4	-3734.966747	1.157153	-3733.753	0.140665	-3733.881739	-3738.579265
S_INT1	**-3462.291993**	**0.993917**	**-3461.2481**	**0.128867**	**-3461.365557**	**-3465.616412**
S_INT1-c2	-3462.291994	0.99396	-3461.2481	0.128341	-3461.365296	-3465.616419
S_INT1-c3	-3462.291994	0.993964	-3461.2481	0.128316	-3461.365283	-3465.616419
S_INT1-c4	-3462.286385	0.992356	-3461.2435	0.130297	-3461.362003	-3465.605805
S_INT1-c5	-3462.285969	0.992369	-3461.2431	0.130536	-3461.361664	-3465.604732
S_INT1-c6	-3462.285968	0.992411	-3461.2431	0.130038	-3461.361425	-3465.60473
S_INT2	-3734.96001	1.160724	-3733.7417	0.143831	-3733.872768	-3738.591373
S_TS2	-3734.956428	1.15611	-3733.7433	0.142976	-3733.873321	-3738.580894
S_INT3	-3734.970885	1.158884	-3733.7541	0.146624	-3733.886356	-3738.59762
S_TS2-c2	-3734.945456	1.155714	-3733.7321	0.146605	-3733.864071	-3738.56761
S_TS2-c2-est	-3734.94425	1.156427	-3733.7302	0.147425	-3733.862389	-3738.566579
S_TS2-c3-est	-3734.952575	1.156756	-3733.739	0.142842	-3733.868832	-3738.569954
S_TS2-c4-est	-3734.952573	1.156769	-3733.739	0.14281	-3733.868808	-3738.569959
S_TS2-c5-est	-3734.952576	1.156777	-3733.739	0.142758	-3733.868783	-3738.569961
TS_rac	-2939.495147	0.635879	-2938.8209	0.104856	-2938.916572	-2942.048115
rc_solv	-3462.338499	0.990347	-3461.2976	0.131804	-3461.416323	-3465.600893
TS1_solv	-3462.338346	0.990392	-3461.2983	0.128381	-3461.41485	-3465.600797
INT1_solv	-3462.359502	0.992335	-3461.3168	0.129777	-3461.434799	-3465.617814

4.3 References

Full reference for Gaussian software:

Gaussian 16, Revision B.01, Frisch, M. J.; Trucks, G. W.; Schlegel, H. B.; Scuseria, G. E.; Robb, M. A.; Cheeseman, J. R.; Scalmani, G.; Barone, V.; Mennucci, B.; Petersson, G. A.; Nakatsuji, H.; Caricato, M.; Li, X.; Hratchian, H. P.; Izmaylov, A. F.; Bloino, J.; Zheng, G.; Sonnenberg, J. L.; Hada, M.; Ehara, M.; Toyota, K.; Fukuda, R.; Hasegawa, J.; Ishida, M.; Nakajima, T.; Honda, Y.; Kitao, O.; Nakai, H.; Vreven, T.; Montgomery Jr., J. A.; Peralta, J. E.; Ogliaro, F.; Bearpark, M.; Heyd, J. J.; Brothers, E.; Kudin, K. N.; Staroverov, V. N.; Kobayashi, R.; Normand, J.; Raghavachari, K.; Rendell, A.; Burant, J. C.; Iyengar, S. S.; Tomasi, J.; Cossi, M.; Rega, N.; Millam, J. M.; Klene, M.; Knox, J. E.; Cross, J. B.; Bakken, V.; Adamo, C.; Jaramillo, J.; Gomperts, R.; Stratmann, R. E.; Yazyev, O.; Austin, A. J.; Cammi, R.; Pomelli, C.; Ochterski, J. W.; Martin, R. L.; Morokuma, K.; Zakrzewski, V. G.; Voth, G. A.; Salvador, P.; Dannenberg, J. J.; Dapprich, S.; Daniels, A. D.; Farkas, Ö.; Foresman, J. B.; Ortiz, J. V; Cioslowski, J.; Fox, D. J. Gaussian, Inc., Wallingford CT, 2016.

[1] M. Gao, D. Kong, A. Clearfield, K. D. Miller, G. W. Sledge, Q.-H. Zheng, Synthesis of carbon-11 labeled triphenylacetamides as novel potential PET melanoma cancer imaging agents. *Synthesis* **2006**, *2006*, 2301–2304.

[2] S. Gaspa, I. Raposo, L. Pereira, G. Mulas, P. C. Ricci, A. Porcheddu, L. De Luca, Visible light-induced transformation of aldehydes to esters, carboxylic anhydrides and amides. *New J. Chem.* **2019**, *43*, 10711–10715.

[3] M. Kou, Z. Wei, Z. Li, B. Xu, Copper-catalyzed sulfinyl cross-coupling reaction of sulfinamides. *Org. Lett.* **2022**, *24*, 8514–8519.

[4] Y. Aota, T. Kano, K. Maruoka, Asymmetric synthesis of chiral sulfoximines through the *S*-alkylation of sulfinamides. *Angew. Chem. Int. Ed.* **2019**, *58*, 17661–17665.

[5] P. Wu, J. Demaerel, B. J. Statham, C. Bolm, Azasulfur(IV) derivatives of sulfite and sulfinate esters by formal S–S bond insertion of dichloramines. *Chem. Sci.* **2024**, *15*, 5333–5339.

[6] S. Tsuzuki, T. Kano, Asymmetric synthesis of chiral sulfimides through the *O*-alkylation of enantioenriched sulfinamides and addition of carbon nucleophiles. *Angew. Chem. Int. Ed.* **2023**, *62*, e202300637.

[7] A. T. Champlin, N. Y. Kwon, J. A. Ellman, Enantioselective *S*-alkylation of sulfenamides by phase-transfer catalysis. *Angew. Chem. Int. Ed.* **2024**, e202408820.

[8] Y. Aota, T. Kano, K. Maruoka, Asymmetric synthesis of chiral sulfoximines via the S-arylation of sulfinamides. *J. Am. Chem. Soc.* **2019**, *141*, 19263–19268.

[9] C. M. M. Hendriks, R. A. Bohmann, M. Bohlem, C. Bolm, *N*-Alkylations of NH-sulfoximines and NH-sulfondiimines with alkyl halides mediated by potassium hydroxide in dimethyl sulfoxide. *Adv. Synth. Catal.* **2014**, *356*, 1847–1852.

[10] S. Gupta, S. Baranwal, N. Muniyappan, S. Sabiah, J. Kandasamy, Copper-catalyzed *N*-arylation of sulfoximines with arylboronic acids under mild conditions. *Synthesis* **2019**, *51*, 2171–2182.

[11] F. Teng, J. Cheng, C. Bolm, Silver-mediated *N*-trifluoromethylation of sulfoximines. *Org. Lett.* **2015**, *17*, 3166–3169.

[12] C. Bohnen, C. Bolm, *N*-Trifluoromethylthiolated sulfoximines. *Org. Lett.* **2015**, *17*, 3011–3013.

[13] X. Zou, H. Wang, B. Gao, Synthesis of sulfoximines by copper-catalyzed oxidative coupling of sulfinamides and aryl boronic acids. *Org. Lett.* **2023**, *25*, 7656–7660.

[14] M. R. Yadav, R. K. Rit, A. K. Sahoo, Sulfoximines: a reusable directing group for chemo- and regioselective ortho C-H oxidation of arenes. *Chem. Eur. J.* **2012**, *18*, 5541–5545.

[15] J. T. Liu, D. S. Brandes, N. S. Greenwood, J. A. Ellman, Synthesis of *N*-acylsulfenamides from amides and *N*-thiosuccinimides. *Synthesis* **2022**, *55*, 2353–2360.

[16] K. Teng, Q. Liu, M. Zhang, H. Naz, P. Zheng, X. Wu, Y. R. Chi, Design and enantioselective synthesis of chiral pyranone fused indole derivatives with antibacterial activities against *Xanthomonas oryzae* pv. *oryzae* for protection of rice. *J. Agric. Food Chem.* **2024**, *72*, 4622–4629.

[17] C. Bannwarth, S. Ehlert, S. Grimme, GFN$_2$-XTB - An accurate and broadly parametrized self-consistent tight-binding quantum chemical method with multipole electrostatics and density-dependent dispersion contributions. *J. Chem.*

Theory Comput. **2019**, *15*, 1652–1671.

[18] S. Grimme, C. Bannwarth, P. Shushkov, A robust and accurate tight-binding quantum chemical method for structures, vibrational frequencies, and noncovalent interactions of large molecular systems parametrized for all spd-block elements (Z = 1-86). *J. Chem. Theory Comput.* **2017**, *13*, 1989–2009.

[19] C. Bannwarth, E. Caldeweyher, S. Ehlert, A. Hansen, P. Pracht, J. Seibert, S. Spicher, S. Grimme, Extended tight-binding quantum chemistry methods. *Wiley Interdiscip. Rev. Comput. Mol. Sci.* **2021**, *11*, e1493.

[20] S. Grimme, Exploration of chemical compound, conformer, and reaction space with meta-dynamics simulations based on tight-binding quantum chemical calculations. *J. Chem. Theory Comput.* **2019**, *15*, 2847–2862.

[21] P. Pracht, F. Bohle, S. Grimme, Automated exploration of the low-energy chemical space with fast quantum chemical methods. *Phys. Chem. Chem. Phys.* **2020**, *22*, 7169–7192.

[22] F. Weigend, R. Ahlrichs, Balanced basis sets of split valence, triple zeta valence and quadruple zeta valence quality for H to Rn: design and assessment of accuracy. *Phys. Chem. Chem. Phys.* **2005**, *7*, 3297–3305.

[23] A. Hellweg, D. Rappoport, Development of new auxiliary basis functions of the karlsruhe segmented contracted basis sets including diffuse basis functions (Def2-SVPD, Def2-TZVPPD, and Def2-QVPPD) for RI-MP2 and RI-CC calculations. *Phys. Chem. Chem. Phys.* **2014**, *17*, 1010–1017.

[24] F. Weigend, Accurate coulomb-fitting basis sets for H to Rn. *Phys. Chem. Chem. Phys.* **2006**, *8*, 1057–1065.

[25] E. R. Davidson, D. Feller, Basis set selection for molecular calculations. *Chem. Rev.* **1986**, *86*, 681–696.

[26] B. J. Lynch, Y. Zhao, D. G. Truhlar, Effectiveness of diffuse basis functions for calculating relative energies by density functional theory. *J. Phys. Chem. A* **2003**, *107*, 1384–1388.

[27] E. Papajak, J. Zheng, X. Xu, H. R. Leverentz, D. G. Truhlar, Perspectives on basis sets beautiful: seasonal plantings of diffuse basis functions. *J. Chem. Theory Comput.* **2011**, *7*, 3027–3034.

[28] X. Yang, Y. Xie, J. Xu, S. Ren, B. Mondal, L. Zhou, W. Tian, X. Zhang, L. Hao, Z. Jin, Y. R. Chi, Carbene-catalyzed activation of remote nitrogen atoms of (benz)imidazole-derived aldimines for enantioselective synthesis of heterocycles.

Angew. Chem. Int. Ed. **2021**, *60*, 7906–7912.

[29] R. Song, Y. Liu, P. K. Majhi, P. R. Ng, L. Hao, J. Xu, W. Tian, L. Zhang, H. Liu, X. Zhang, Y. R. Chi, Enantioselective modification of sulfonamides and sulfonamide-containing drugs: via carbene organic catalysis. *Org. Chem. Front.* **2021**, *8*, 2413–2419.

[30] Y. Lv, G. Luo, Q. Liu, Z. Jin, X. Zhang, Y. R. Chi, Catalytic atroposelective synthesis of axially chiral benzonitriles via chirality control during bond dissociation and CN group formation. *Nat. Commun.* **2022**, *13*, 1–9.

[31] R. Deng, S. Wu, C. Mou, J. Liu, P. Zheng, X. Zhang, Y. R. Chi, Carbene-catalyzed enantioselective sulfonylation of enone aryl aldehydes: a new mode of breslow intermediate oxidation. *J. Am. Chem. Soc.* **2022**, *144*, 5441–5449.

[32] W. X. Lv, H. Chen, X. Zhang, C. C. Ho, Y. Liu, S. Wu, H. Wang, Z. Jin, Y. R. Chi, Programmable selective acylation of saccharides mediated by carbene and boronic acid. *Chem* **2022**, *8*, 1518–1534.

[33] X. Yang, L. Wei, Y. Wu, L. Zhou, X. Zhang, Y. R. Chi, Atroposelective access to 1,3-oxazepine-containing bridged biaryls via carbene-catalyzed desymmetrization of imines. *Angew. Chem. Int. Ed.* **2022**, *62*, e202211977.

[34] Z. Luo, M. Liao, W. Li, S. Zhao, K. Tang, P. Zheng, Y. R. Chi, X. Zhang, X. Wu, Ionic hydrogen bond-assisted catalytic construction of nitrogen stereogenic center via formal desymmetrization of remote diols. *Angew. Chem. Int. Ed.* **2024**, e202404979.

[35] J. Zheng, H. Feng, X. Zhang, J. Zheng, J. K. W. Ng, S. Wang, N. Hadjichristidis, Z. Li, Advancing recyclable thermosets through C═C/C═N dynamic covalent metathesis chemistry. *J. Am. Chem. Soc.* **2024**, *146*, 21612–21622.

[36] D. Liu, T. Tu, T. Zhang, G. Nie, T. Liao, S.-C. Ren, X. Zhang, Y. R. Chi, Photocatalytic direct para-selective C−H amination of benzyl alcohols: selectivity independent of side substituents. *Angew. Chem. Int. Ed.* **2024**, e202407293.

[37] B. Li, J. Hu, M. Liao, Q. Xiong, Y. Zhang, Y. R. Chi, X. Zhang, X. Wu, Catalyst control over S(IV)-stereogenicity via carbene-derived sulfinyl azolium intermediates. *J. Am. Chem. Soc.* **2024**, *146*, 25350–25360.

[38] K. Fukui, Formulation of the reaction coordinate. *J. Phys. Chem.* **2005**, *74*, 4161–4163.

[39] K. Fukui, The path of chemical reactions - the IRC approach. *Acc. Chem. Res.* **1981**, *14*, 363–368.

[40] J. M. Goodman, M. A. Silva, QRC: A rapid method for connecting transition structures to reactants in the computational analysis of organic reactivity. *Tetrahedron Lett.* **2003**, *44*, 8233–8236.

[41] V. S. Bryantsev, M. S. Diallo, W. A. Goddard Iii, W. A. Goddard, Calculation of solvation free energies of charged solutes using mixed cluster/continuum models. *J. Phys. Chem. B* **2008**, *112*, 9709–9719.

[42] B. T. Boyle, J. N. Levy, L. De Lescure, R. S. Paton, A. McNally, Halogenation of the 3-position of pyridines through zincke imine intermediates. *Science* **2022**, *378*, 773–779.

[43] A. Darù, X. Hu, J. N. Harvey, Iron-catalyzed reductive coupling of alkyl iodides with alkynes to yield cis-olefins: mechanistic insights from computation. *ACS Omega* **2020**, *5*, 1586–1594.

[44] G. Luchini, J. V. Alegre-Requena, I. Funes-Ardoiz, R. S. Paton, GoodVibes: Automated thermochemistry for heterogeneous computational chemistry data. *F1000Research* **2020**, *9*, 291.

[45] L. Schrödinger, The PyMOL molecular graphics development component. *Version 1.8*; **2015**.

[46] S. Xiong, M. M. Shoshani, X. Zhang, H. A. Spinney, A. J. Nett, B. S. Henderson, T. F. T. Miller, Agapie, Efficient copolymerization of acrylate and ethylene with neutral P, O-chelated nickel catalysts: mechanistic investigations of monomer insertion and chelate formation. *J. Am. Chem. Soc.* **2021**, *143*, 6516–6527.

[47] L. Wei, J. Li, Y. Zhao, Q. Zhou, Z. Wei, Y. Chen, X. Zhang, X. Yang, Chiral phosphoric acid catalyzed asymmetric hydrolysis of biaryl oxazepines for the synthesis of axially chiral biaryl amino phenol derivatives. *Angew. Chem. Int. Ed.* **2023**, *62*, e202306864.

[48] J. Das, W. Ali, A. Ghosh, T. Pal, A. Mandal, C. Teja, S. Dutta, R. Pothikumar, H. Ge, X. Zhang, D. Maiti, Access to unsaturated bicyclic lactones by overriding conventional C(Sp^3)–H site selectivity. *Nat. Chem.* **2023**, 1–10.

[49] S. Kozuch, S. Shaik, How to conceptualize catalytic cycles? the energetic span model. *Acc. Chem. Res.* **2011**, *44*, 101–110.